MIMIC

A New Approach to Visualizing Satellite Microwave Imagery of Tropical Cyclones

BY ANTHONY J. WIMMERS AND CHRISTOPHER S. VELDEN

Sequential satellite microwave images of tropical cyclones readily lend themselves to morphing applications, which allow for a straightforward visualization of the storms' structural trends.

Polar and other low-Earth-orbiting (LEO) satellites provide critical data for use in weather analysis and forecasting. However, the temporal sampling issue leads to the common problem of interpreting sequential images spaced at irregular and sometimes very lengthy time intervals. LEO microwave imagery of tropical cyclones is one of the most extreme cases of this problem, because not only are the weather systems moving, but also the LEO spatial coverage gaps are largest in the Tropics. As a result, the temporal image spacing can range from less than 30 min to more than 25 h, although the more typical spacing tends to vary between 3 and 6 h.

AFFILIATIONS: WIMMERS AND VELDEN—Cooperative Institute for Meteorological Satellite Research (CIMSS), University of Wisconsin—Madison, Madison, Wisconsin
A supplement to this article is available online (DOI:10.1175/BAMS-88-8-Wimmers)
CORRESPONDING AUTHOR: Anthony J. Wimmers, CIMSS, 1225 W. Dayton St., Madison, WI 53706
E-mail: wimmers@ssec.wisc.edu

The abstract for this article can be found in this issue, following the table of contents.
DOI:10.1175/BAMS-88-8-1187

In final form 19 March 2007

Unlike geostationary satellite imagery that is updated frequently, forecasters often acknowledge the difficulty of mentally piecing together a recent history of a tropical cyclone from these irregular LEO datasets. Specifically, the time sensitivity of the interpretation process adds uncertainty to their conclusions on, for example, short-term structural changes. In tropical cyclone applications, the LEO microwave imagery can provide unique information on convective organization, secondary eyewall formation, and eyewall replacement cycles, all of which is critical information when trying to forecast intensity changes (Cecil and Zipser 1999; Jones et al. 2006; Houze et al. 2006). This information is usually lacking in the geostationary channels because of obstructing cloud tops. Clearly, the analysis of tropical cyclones undergoing rapid fluctuations in structure and intensity should benefit greatly from a time-continuous visualization of the LEO microwave imagery.

Our approach is to blend sequential individual LEO microwave images together through a "morphing" process, which is the digital manipulation of two or more images to make them appear to change into one another naturally. This approach has been explored in the field of digital image processing for well over a decade [see Ruprecht and Müller (1995) and Wolberg (1998) for good overviews on morphing]. It has been

applied more recently to meteorological imagery by the National Oceanic and Atmospheric Administration/National Weather Service (NOAA/NWS) using the Climate Prediction Center (CPC) Morphing Technique (CMORPH) software (Joyce et al. 2004), wherein microwave rainfall retrievals are blended together by advection with satellite-derived midtropospheric cloud-drift winds. A related approach is the linear extrapolation of moving precipitation fields, such as with sequential radar imagery (Hohti et al. 2000; Germann and Zawadzki 2002) or satellite microwave-derived precipitation using geostationary cloud-drift winds (Grose et al. 2002).

In this paper we introduce a novel morphing algorithm called the Morphed Integrated Microwave Imagery at the Cooperative Institute for Meteorological Satellite Studies (CIMSS) (MIMIC) that can be used to improve the visualization of tropical cyclones, which in turn should enhance the ability to analyze and forecast these events. This algorithm is used to create the following two products described herein: MIMIC-TC presents a tropical cyclone–centered LEO microwave imagery animation, and MIMIC-IR animates a tropical cyclone–retrieved precipitation field layered over geostationary infrared imagery. Several examples in this paper have supplemental movies, which can be found online at http://dx.doi.org/10.1175/BAMS-88-8-Wimmers). In addition, we maintain an experimental real-time Web site for the MIMIC-TC and MIMIC-IR products online at http://cimss.ssec.wisc.edu/mimic.

THE MIMIC-TC MORPHING TECHNIQUE.

The ultimate goal of MIMIC-TC is to create a smooth animation from sequential but irregularly spaced microwave imagery produced from multiple LEO satellites overflying a target tropical cyclone. MIMIC-TC incorporates 85–92-GHz microwave data from six LEO satellites (Table 1) in near–real time as the data become available. [The Advanced Microwave Sounding Unit-B (AMSU-B) instrument is not currently used because of the difficulty in incorporating imagery with its low resolution and changing polarization with zenith angle; however, it may be included in the future.] The signal from these channels is strongly attenuated by large hydrometeors (~2-mm diameter and greater) generated by deep convection (Spencer et al. 1989; Grody 1993), and therefore the imagery is often used as a proxy for the distribution of precipitation in tropical cyclones. The microwave signal can penetrate through obstructing ice clouds that are common in tropical cyclones and uniquely reveal the structure of the eyewall and organization of the spiral bands (Hawkins et al. 2001; Lee et al. 2002; Houze et al. 2006). Because the various LEO satellite instruments employed by MIMIC-TC have slightly different response functions and calibrations, it is necessary to perform an empirical adjustment to the brightness temperatures to minimize any differences and improve the visualization. This normalization process is described in the appendix. In order to ensure proper navigation, the algorithm uses only swaths that contain the center of the TC rotation. The final product is interpolated to a polar coordinate grid around the center of rotation (2.78-km radial resolution and 1° angular resolution), which facilitates the computation of angular motion.

When blending sequential microwave images of a tropical cyclone, the morphing algorithm must balance two contending trends. The first trend is the cyclonic advection of convective signals within the circulation of the storm, which can be roughly approximated as radially symmetric motion in a

Table 1. Satellite microwave instruments that contribute to the MIMIC-TC product.

Satellite	Instrument	Frequency (GHz)	Orbit	Footprint (km)	References
DMSP-13*	SSM/I	85.5 H**	Polar, sun synchronous	16 × 14	Raytheon (2000)
DMSP-14	SSM/I	85.5, H	Polar, sun synchronous	16 × 14	"
DMSP-15	SSM/I	85.5, H	Polar, sun synchronous	16 × 14	"
DMSP-16	SSMIS	91.7, H	Polar, sun synchronous	14 × 13	NOAA OSDPD (2002)
TRMM	TMI	85.5, H	Equatorial, between 38°S and 38°N	7 × 5	Kummerow et al. (1998)
Aqua	AMSR-E	89.0, H	Polar, sun synchronous	6 × 4	NASA MSFC (2001)

*DMSP: Defense Meteorological Satellite Program

**H: Horizontal polarization

storm-centered frame of reference. This motion is also observed in conventional surface-based radar animations at smaller scales (~20 km) as individual precipitation features advect with the vortex flow. An example can be found in the movie for Hurricane Katrina (2005) in the following section. The second trend is the development of larger organized convective events, which are usually driven by forces that are not directly foretold in the microwave imagery—diabatic heating, localized convergence, shear, etc. An example is the formation of an eyewall. As opposed to the first trend (advection), the organized convection trend can appear to be quasi stationary and/or not dictated by the rotational winds. In order to address both trends, the algorithm employs what we call a "rotating fade" within a cyclone-centered frame of reference.[1] This process is demonstrated in Fig. 1 and supplemental animation 1 (http://dx.doi.org/10.1175/BAMS-88-8-Wimmers).

The rotation component of the algorithm is a radial wind loosely based on a tropical cyclone wind profile (Holland 1980) for an average well-organized storm (with a major modification for the radial winds in the vicinity of the eyewall) scaled by the estimated maximum sustained surface winds reported by the Joint Typhoon Warning Center or the National Hurricane Center (Fig. 2). This function has three principal elements. First, the eyewall region does not have a rotational component, recognizing that the observed trends in the established eyewall at

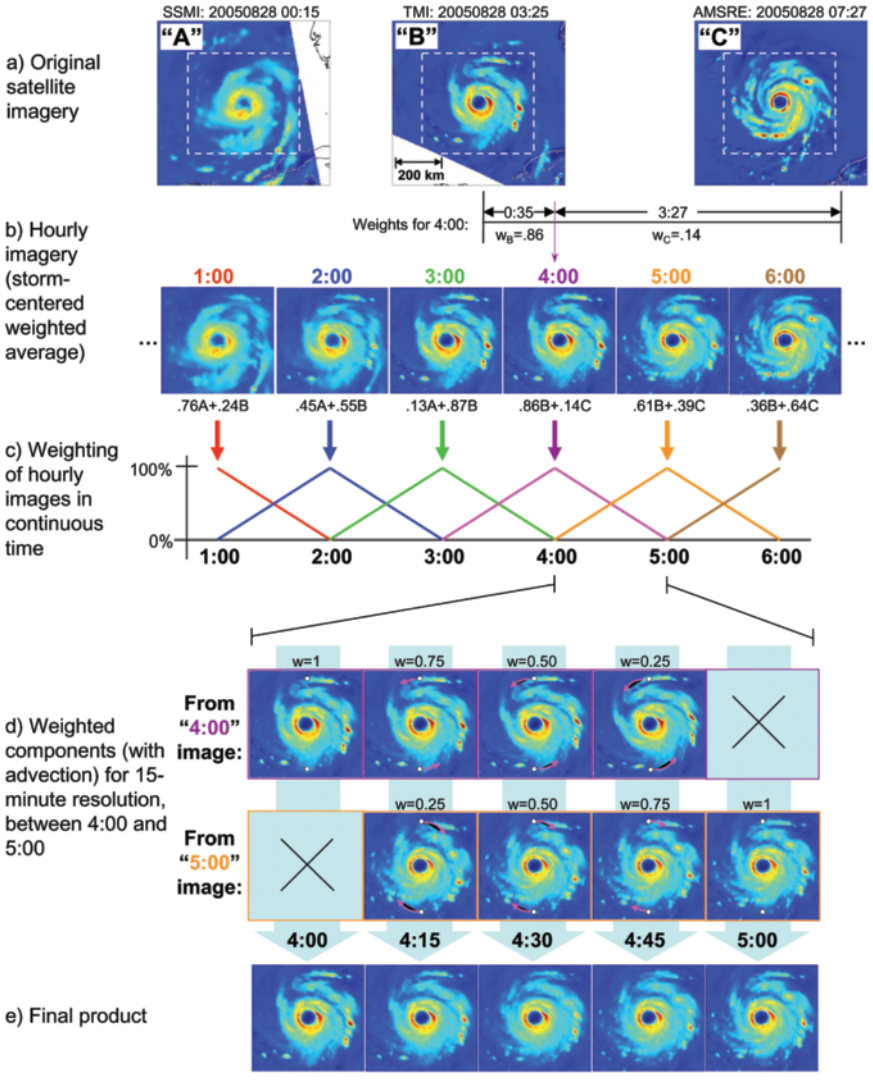

Fig. 1. The steps of the MIMIC-TC algorithm. The morphing process is shown for a 5-h time interval between three satellite overpasses (a) of Hurricane Katrina. The dashed boxes in (a) indicate the detail that is shown in the subsequent steps. (b) Intermediate images are created at each hour from a simple time-weighted average of the nearest storm-centered images before and after the hour. (c) The algorithm uses each intermediate image in an overlapping 2-h period. (d) Within the span of an hour, the earlier intermediate image is rotated forward from its original time and blended into the later image, which is rotated forward toward *its* original time. Arrows indicate the direction of the advection function. (e) These two components are weighted linearly such that the earlier image rotates and fades into the later image in the final product. Note the following changes over time in the final product: more convection emerges on the southwestern side of the image, convective cells on the eastern side of the "4:00" image move cyclonically and are replenished by cells from the "5:00" image, and the inner spiral band on the western side weakens. The full-length animation of the MIMIC-TC product created from these three original microwave images can be seen in supplemental animation 1.

[1] When the algorithm runs in real time, we employ an automated center-fixing scheme that will be described in a subsequent paper.

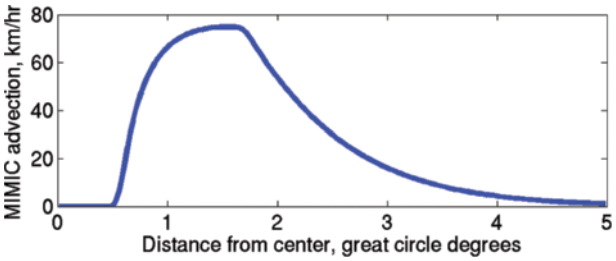

FIG. 2. MIMIC-TC advection function for a TC with maximum sustained winds (Vmax) of 100 kt. For Vmax = 50 kt, the function is scaled by 0.5, and so on.

the scale of the microwave imagery are principally nonadvective. That is, radially symmetric eyewalls as viewed in the microwave imagery have no need for rotational operations, and asymmetric eyewalls are often asymmetric resulting from the effects of vertical wind shear. Vertical wind shear is a change in the environmental wind speed or direction with height, which can cause disorganization in the storm structure. During an episode of significant vertical shear, more intense convection normally occurs on the downshear side of the storm core (Corbosiero and Molinari 2002). This can appear as a quasi-static asymmetric eyewall signature in the low-resolution microwave imagery, even though in reality the individual convective cells rotate with the vortex flow.

Second, the advection function outside the eyewall peaks at a distance of about 1.5° from the rotation center; this models the transitional zone in which inner spiral bands experience strong horizontal shear and converge toward the eyewall (Rozoff et al. 2006). Also, the advection function at this distance can capture the motion along a secondary eyewall (if present) while retaining the position of any identifiable asymmetries. Third, the tail of the advection function approximates the asymptotic decrease of wind with distance from the Holland profile. Given these parameters, we understand that this advection function is hardly optimized for every tropical cyclone, but 2 yr of experience show that this function is suitable for most storms, and it is especially well suited to cases in which the center of rotation is well established, which is normally in strong tropical storm strength TCs and higher (see information online at MIMIC's Web site; http://cimss.ssec.wisc.edu/mimic.[2] One principal drawback, of course, is the absence of a radial component of motion, which is more difficult to generalize and is discussed more in the following sections.

The advantage of the rotating fade is that it applies differently at varying scales. At the scale of individual convective cells, it shows those cells to be moving cyclonically with the vortex wind. In the typical fashion for tropical cyclones, these regions of cells emerge from the same convergent areas and generally show a life span of about 2 h (confirmed by land-based radar observations). On the other hand, large regions of convection (>100 km), including the eyewall, outer spiral bands, and both organized and disorganized areas within the closed rotation of the cyclone, are mostly unperturbed by the advection scheme. These areas are subject to change only from the fading scheme, where one microwave image fades into another.

There are two main drawbacks to this process. The first is the unavoidable case in which the raw microwave imagery does not update often enough, which results in one image fading unrealistically into the next, for example, a spiral band disappears from one place and reappears in another, or the eyewall changes the orientation of its asymmetry without apparent cause. Although this effect can be quite unnatural, the user can often compensate for the misrepresentation and interpret the underlying phenomenon correctly. Specifically, in the case of the disappearing and reappearing spiral band, the user understands implicitly that the band is simply moving from one position to another. Likewise, the changing orientation of the asymmetry of an eyewall is obviously a gradual angular displacement. However, in some cases, the time gap between microwave images is so great that neither an algorithm nor a trained analyst can easily discern the pattern of change between the two images.

The second main drawback is an effect we call "pulsing," which occurs when well-defined convective cells outside of the eyewall advect rapidly and appear to regenerate in place. This occurs because the rotating fade is not the best-suited scheme for convective cells near the eyewall, which are more likely to evolve over time by shearing or entrainment into the eyewall(s). Fortunately again, when the user is aware of this effect, the artifact is more of an annoyance, and it is relatively easy to incorporate this knowledge into the interpretation of the animation.

MIMIC-TC EXAMPLES AND VALIDATION.

The best option for validation of MIMIC-TC is a direct comparison to ground-based coastal radars.

[2] Readers are encouraged to visit the MIMIC real-time Web site listed above to view an archive of over 100 TCs from 2004 to the present, which include a wide variety of TCs over their entire life spans. This will give readers a more complete impression of the workings of this morphing technique beyond what we are able to present in the few examples in this paper.

The approach we take is through side-by-side comparison with contemporaneous radar animations to determine whether the end user will draw the same conclusions from both. The reasons for a qualitative rather than a quantitative comparison will become clear as the two products depict the same components of the TCs (eyewall dynamics, distribution of convection, etc.) but in physically different ways.

The Atlantic hurricane event from 2005 with the best radar coverage was Wilma as it passed through Florida on 24 October (Fig. 3, supplemental animation 2 online at http://dx.doi.org/10.1175/BAMS-88-8-Wimmers). Most of Wilma remains in the short- range view (<230 km) of four radar stations between 0600 and 1800 UTC. Shown side by side, MIMIC-TC and ground-level radar present the same histories of the storm structure as it crosses Florida. Both show that the strongest convection within Wilma is predominantly to the north of the eyewall. Between 0600 and 1400 UTC both the microwave scattering and radar reflectivity are stronger on the northern side of the eyewall, while a dry slot develops to the southwest. In both sequences, the eye expands and becomes less organized as it crosses into the Atlantic around 1500 UTC. Also at this time, both animations show the intensification of the eyewall on the trailing side of the storm, which was responsible for much of the property damage in eastern Florida. One significant difference between the two animations is that MIMIC-TC shows a well-defined spiral band on the eastern side of Wilma, and although the radar shows filaments of precipitation in the same area, the radar does not show a persistent eastern band like that in MIMIC-TC.

The MIMIC-TC Wilma animation shows the artifacts that result from blending images in the vicinity of a coastal boundary, which in this case is the west coast of Florida. Notice how the Florida peninsula (dark blue) appears to move with respect to the coastline overlay. Fortunately, this artifact is easily distinguishable from convection, and only occurs away from the areas of ice scattering. Also, the north-northwestern inner band exhibits a good example of pulsing (discussed in the previous section) between 0600 and 1300 UTC.

The MIMIC-TC and radar animations for Hurricane Katrina (Fig. 4, supplemental animation 3 online at http://dx.doi.org/BAMS-88-8-Wimmers) show another recent case of a major tropical cyclone at landfall. Both products capture the arrival of a northern outer band around 0000 UTC 29 August 2005, subsequently weakening from west to east. A second band brings a succession of small convective cells (~20 km each in size) to southern Louisiana around 0400 UTC and to the Mississippi coast around 0600 UTC. Many of the individual cells in that band are tracked in the radar animation, and we note that they have lifetimes of about 2 h, just as with the parameterized depiction of the MIMIC-TC product. A large dry slot is apparent in the western sector in both animations starting around 0900 UTC, but it is larger and grows more continuously in MIMIC-TC than in the radar, and by 1600 UTC the radar shows precipitation over Lake Ponchartrain (30.2°N, 90.2°W) but MIMIC-TC shows no activity. This is either because of advection and dispersion of precipitation at lower levels in the cyclone into the dry zone, or because of lower-intensity stratiform precipitation, both of which are detected in the radar but not as prominently in microwave imagery.

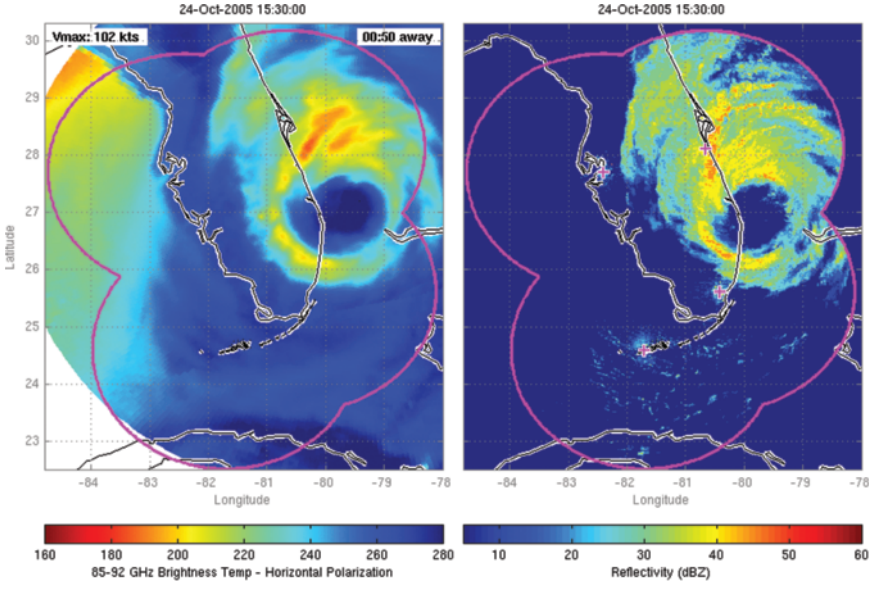

Fig. 3. (left) MIMIC-TC and (right) NEXRAD composite radar base reflectivity for 1530 UTC 24 Oct 2005 depicting Wilma crossing Florida. The labels are as follows: (top left) NHC-reported maximum sustained winds interpolated in time, (top right) the temporal separation from the microwave overpass nearest in time (either before or after); radar composite domain, magenta perimeter; radar station positions, magenta "+." Supplemental animation 2 addresses this figure.

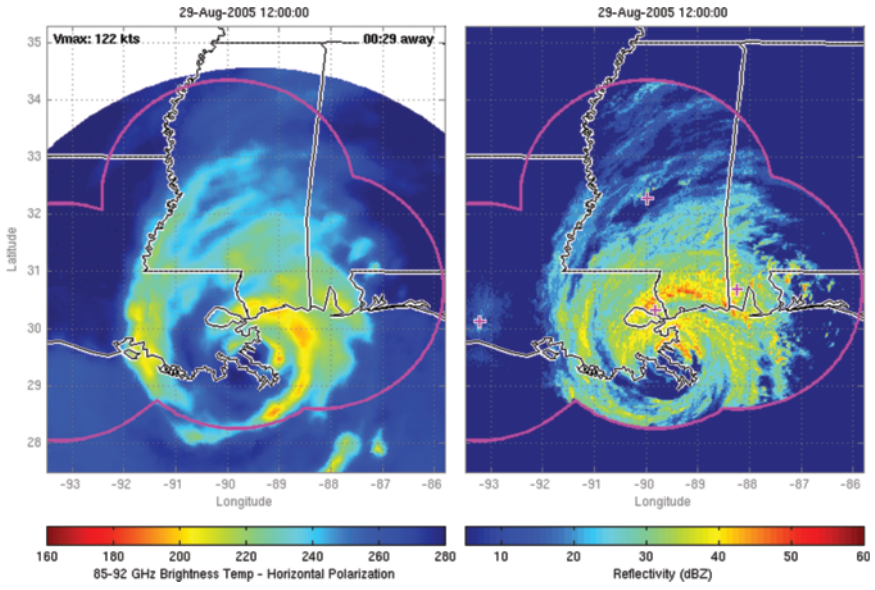

Fig. 4. (left) MIMIC-TC and (right) NEXRAD composite radar base reflectivity for 1200 UTC 29 Aug 2005 depicting Katrina's landfall on the Gulf Coast. The labels are as in Fig. 3. Supplemental animation 3 addresses this figure.

Katrina's inner and outer eyewalls are well defined in the MIMIC-TC animation, which shows that Katrina's outer eyewall has a nearly continuous ring of convection (with some breaks in the ring to the south) during landfall on the Mississippi River delta (~0600 UTC). As the storm center moved across Louisiana and up along the Louisiana–Mississippi border, the convection weakens on the southwestern side of the outer eye, but the northern half remains well defined until about 1600 UTC as the storm tracked across Louisiana and into Mississippi. Likewise, the inner eyewall begins as a closed ring of convection before landfall, but convection weakens on the southwest side such that the inner eyewall takes a crescent shape around 1000 UTC. Subsequently, the eastern eyewall shows increased convective intensity during landfall on the Mississippi coast at 1400 UTC before becoming disorganized farther inland. In contrast, the coincident radar animation shows intermittent banding of precipitation around the outer eyewall, and it is apparent only after several hours of radar animation that this area produces an overall secondary maximum of precipitation. Thus, the existence and timing of the outer eyewall at landfall is less certain in the radar than in MIMIC-TC. The inner eyewall is well defined in the radar because of its continuous localized maximum in precipitation, and the timing of the southwest weakening during landfall in Louisiana and the relative strength on the eastern side during landfall in Mississippi are in agreement with the trends in MIMIC-TC.

A more complete representation of an eyewall replacement cycle (ERC; Fortner 1958; Willoughby et al. 1982) is captured in the MIMIC-TC animation of Hurricane Ivan (2004; supplemental animation 4 online at http://dx.doi.org/10.1175/BAMS-88-8-Wimmers). This sequence follows Ivan during its first of two ERCs and its brush with Jamaica (from 1200 UTC 10 September to 1200 UTC 11 September). This animation clearly depicts not only the emergence of the secondary eyewall and the subsequent decay of the inner eyewall, but it also depicts how these events transpired within the erratic

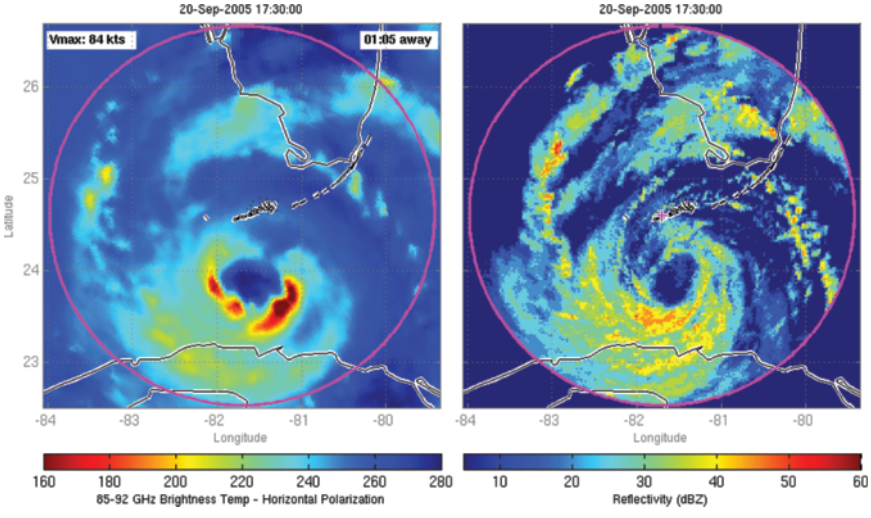

Fig. 5. (left) MIMIC-TC and (right) NEXRAD composite radar base reflectivity for 1730 UTC 20 Sep 2005 depicting Rita passing south of Key West. The labels are as in Fig. 3. Supplemental animation 4 addresses this figure.

track of the storm over that time (consistent with the National Hurricane Center best-track path) in conjunction with its encounter with Jamaica.

Finally, an example from Hurricane Rita (2005) was chosen because it is effective at showing the limitations of the MIMIC-TC product (Fig. 5, supplemental animation 5 online at http://dx.doi/10.1175/BAMS-88-8-Wimmers). As in the other examples, the MIMIC-TC depiction matches radar in depicting the overall behavior of the storm structure. However, the eyewall is depicted somewhat differently in the two products. In MIMIC-TC, the eyewall is a shifting assortment of convective cells, whereas in the radar, the eyewall is made up of thin, curved precipitation filaments with considerably shorter lifetimes. The eyewall does not achieve a closed ring of convection until approximately 0000 UTC 20 September, and before that time the radar shows that the irregularity in the eyewall shifts and rotates quickly with the entrainment of inner bands and advection of convective cells. Clearly, the microwave data do not update quickly enough to capture this evolution, and the fade process is not optimal in this case, so inconsistencies exist at the scale of the eyewall (Fig. 5). However, despite the inability to capture details, the MIMIC-TC animation does effectively depict the degree of organization within the eyewall as it increases in radial symmetry toward 0000 UTC 20 September.

Overall, these examples demonstrate the usability of the MIMIC-TC product and provide guidance for interpreting it effectively. By highlighting convection-driven over stratiform precipitation, MIMIC-TC distinctly presents the dominant components of the TC structure (eyewalls, bands) and behavior (trends, secondary eyewall formation, eyewall replacement cycles). However, in many cases the limited spatial resolution of the microwave imagery prevents the observation of very small (subpixel) eyes and finer convective filaments that connect the inner rainbands to the eyewall.

Not surprisingly, another general characteristic of the MIMIC-TC product is that its accuracy in depicting the visual continuity of structural changes decreases with the increasing time gap between successive microwave images (displayed as the time "away" in the upper-right corner of the animation). Based on experience from viewing dozens of tropical cyclones, we find that beyond about 3 h from an actual microwave observation, the morphed product begins to lack definition and is less likely to give proper information about eyewall asymmetries and size.

MIMIC-IR. Geostationary infrared imagery and LEO microwave imagery are complementary tools for viewing tropical cyclones, and it is common for tropical cyclone analysts to utilize both to achieve the optimum interpretation of storm position and structure. To this end, an additional visualization tool has been created—MIMIC-IR—which overlays a morphed microwave product onto geostationary infrared imagery. Animation of this combination creates a simultaneous view of precipitation and cloud distribution, and is similar to an overlay of radar onto geostationary imagery.

Table 2. Geostationary satellites used in MIMIC-IR.

Satellite	Nadir longitude	Basin
GOES-East	75°W	North Atlantic
GOES-West	135°W	West Pacific, central Pacific
MTSAT	140°E	East Pacific, central Pacific
Indoex	63°E	Indian Ocean

The microwave imagery used in MIMIC-IR is the polarization-corrected temperature (PCT), which is slightly different from the brightness temperature used in MIMIC-TC. The PCT is computed from a weighted difference between the vertical and horizontal polarizations of the 85–92-GHz frequency, which isolates the signal of precipitation from the surface background (Spencer et al. 1989). (In the MIMIC-TC product, the horizontal polarization brightness temperature is preferred over the PCT because the horizontal polarization shows important textures that indicate the storm's circulation.) The morphing algorithm itself is exactly the same as that of MIMIC-TC described above.

The infrared imagery for MIMIC-IR is taken from the nearest of four possible geostationary satellites (Table 2). The temporal frequency of these satellites' images is normally between 15 and 60 min, although each experiences an occasional data blackout (either because of an eclipse period or because of technical issues), which causes longer gaps in the data availability. The infrared image shown in the MIMIC-IR product is the one closest in time to the display time (either before or after). In contrast to the morphed microwave product, the infrared imagery is always displayed in its original position at the image time stamp and is not "nudged" with time to follow

the TC track. This allows the observer to use the infrared image as a reliable validation for the position of matching TC features, as long as the infrared image is updated rapidly (<30-min intervals).

In MIMIC-IR, PCT and infrared are two unique "layers" of imagery. The PCT layer is semitransparent to permit a direct comparison with the underlying infrared image. For example, often an outer spiral band will move rapidly away from the storm center, but the morphed PCT pattern will not follow the true motion apparent in the clouds because the advective scheme does not account for this divergent radial motion. In this case the end user must mentally picture the PCT-resolved convection moving in tandem with the infrared-resolved cloud advection. Using this guideline, the visualization of developing cyclones (before a center of rotation is established) can be substantially improved compared to the MIMIC-TC depiction.

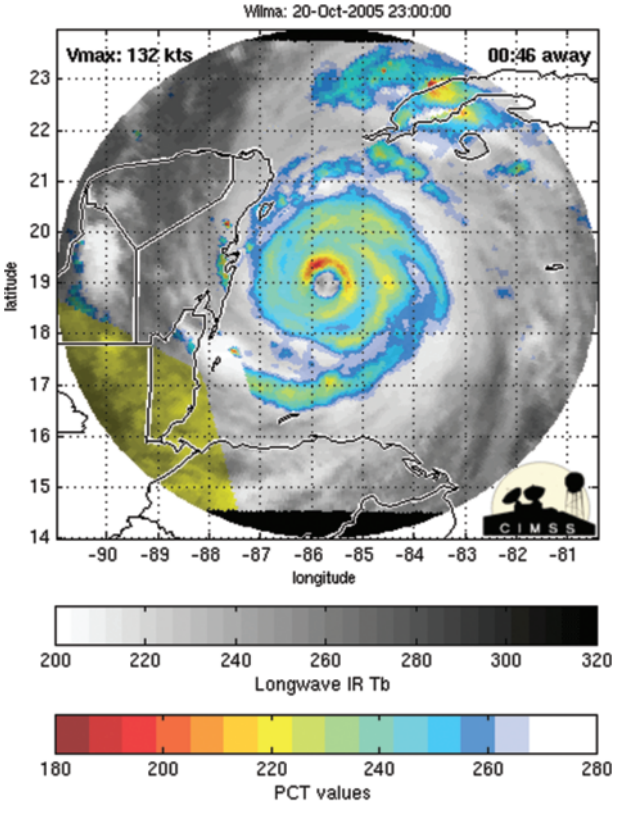

Fig. 6. MIMIC-IR for 2300 UTC 20 Oct showing Hurricane Wilma (2005) approaching the Yucatan peninsula. The infrared layer is the *GOES-12* longwave infrared brightness temperature, adjusted for parallax assuming cloud tops at 15 km and matched to the nearest display time. The PCT layer is semitransparent over the infrared layer, and it is corrected for parallax assuming a signal peak at 7-km height. The semitransparent PCT layer allows breaks in the cloud cap to be seen as a darkening of PCT colors. Solid yellow areas are "no microwave data" regions. The labels are as follows: (top left) NHC-reported maximum sustained winds interpolated in time, (top right) the temporal separation from the microwave overpass nearest in time (either before or after). Supplemental animation 6 addresses this figure.

An example of MIMIC-IR for an earlier sequence of Hurricane Wilma (2005) illustrates the main features of this product (Fig. 6, supplemental animation 6 online at http://dx.doi.org/10.1175/BAMS-88-8-Wimmers). Here the IR imagery clearly shows that the bands farther than about 2.5° (275 km) from the storm center are moving away from the storm. However, inside this radius the convective activity is obscured in the IR by the cirrus cloud cap, and here the PCT reveals the structure of the inner bands, the eyewall, and a secondary eyewall after about 1200 UTC 21 October. In fact, the PCT reveals that the eyewall is consistently ~50 km in diameter for almost 2 days, while the clouds obscure this fact in the IR for most of this time.

CONCLUDING REMARKS. This article introduces a new visualization tool that makes use of morphing techniques to create time-continuous animations of irregular satellite images. Specifically, the MIMIC-TC tool inputs passive microwave imagery from multiple LEO satellite overpasses of a target tropical cyclone and displays a smoothly transitioned movie of the key structure trends. The MIMIC-TC display is especially efficient at visualizing the evolution of banding structures, secondary eyewall formation, and eyewall replacement cycles, all of which are important to the organization and intensity analysis. A derivative of this tool, MIMIC-IR, overlays the microwave signatures onto clouds as depicted in coincident geostationary satellite IR imagery, yielding a multispectral visualization of tropical cyclone behavior.

Many areas still require improvement in order to more fully optimize the MIMIC algorithms. First, the depiction of features "fading" from one position to the next (rather than moving continuously) as well as "pulsing" artifacts should be reduced by introducing more realistic motion. Second, the advection function should be parameterized to match the state (i.e., current size and intensity) of the tropical cyclone. This would require regular input information from tropical analysis centers. Third, a possibility exists to make use of atmospheric modeling methods to allow for more physically based transitions between observations. This would be more difficult to constrain effectively because of the limited amount

of independent data close in time to the satellite overpasses. On the other hand, the product in its current form is totally independent from models, which makes it an effective complement to the model-based forecasts and analyses.

As with every new observational tool, MIMIC requires the user to be familiar with its unique strengths and weaknesses in order to interpret it properly. Given this, a forecaster can follow trends in a tropical cyclone's structure more efficiently and effectively. Ultimately, it is hoped that this improved analysis could result in higher-confidence short-term intensity forecasts.

The subject of morphing tropical cyclone imagery is a fresh topic with many exciting possibilities for visualization, and we see this product as merely a first step. With feedback from the community of users, we anticipate continued improvements over time toward this visualization strategy. Because we are now in the "golden age" of satellite microwave observation, such improvements in visualization will become increasingly important over time.

ACKNOWLEDGMENTS. This work was sponsored by the Oceanographer of the Navy through the PEO C4I PMW-150 program office and the Naval Research Laboratory (Jeff Hawkins). We thank Joe Turk, Jeffrey Tesmer, and Hal Wolf for their kind assistance with microwave data access and decoding. We thank Tom Whittaker for contributing the Java module to read and reformat geostationary imagery. We also thank the reviewers for their constructive advice.

APPENDIX: NORMALIZING BRIGHTNESS TEMPERATURES.

The differences between the corresponding footprint sizes and response functions of each microwave instrument [Special Sensor Microwave Imager (SSM/I), Tropical Rainfall Measuring Mission (TRMM) Microwave Imager (TMI), Advanced Microwave Scanning Radiometer (AMSR)-Earth Observing System (E), Special Sensor Microwave Imager/Sounder (SSMI/S)] impart a noticeable brightness temperature bias in the morphing transitions if the imagery is not normalized to a single standard. To minimize this bias we have developed an empirical correction to the 85–92-GHz horizontally polarized brightness temperatures based on histogram matching (Bovik 2000). In its conventional application, a histogram-matching algorithm adjusts the brightness values of a source image to give it the same brightness value histogram of a target image. This application is preferable to a pixel-to-pixel comparison between different instruments' imagery because the time differences between observations from each orbital platform leads to significant spatial offsets in the features being compared.

The TMI imagery served as the calibration standard because TRMM is the only satellite to regularly cross tracks with the other satellites, and also because its footprint size is between the large and small extremes. Calibration datasets for each imager were selected from six to eight scenes from three tropical cyclones with well-developed eyes. In each scene, a source image matched with a TMI image with a time gap 2 h or less. Both images were interpolated to the storm-centered, polar grid format used in the morphed display. This ensured that the *final,* interpolated images from the respective instruments would show a minimum amount of bias. Pixels were weighted by inverse distance from the center in order to emphasize the importance of matching the brightness temperatures in the eyewall. The resulting adjustments (Fig. A1) show an overall negative adjustment to SSM/I brightness temperatures and an overall positive adjustment to AMSR-E and SSMI/S brightness temperatures in the scattering range (<~270 K). In the "background" range (>~270 K), SSM/I brightness temperatures are adjusted slightly upward, AMSR-E brightness temperatures are downward, and SSMI/S temperatures are basically unaffected.

We hasten to add that a robust normalization of raw brightness temperatures (rather than interpolated values) would yield somewhat different results from those shown here. This is because our normalization gives added weight to the eyewall, and also because matching histograms of interpolated images does not produce the same results as with noninterpolated imagery. Therefore, the adjustments shown here should not be used directly in other applications.

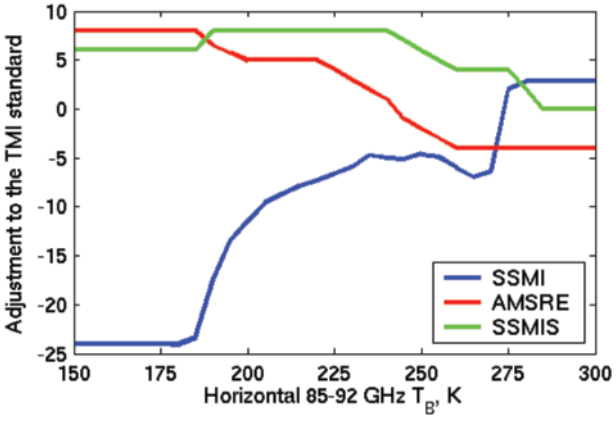

Fig. A1. Adjustments to SSM/I, AMSR-E, and SSMI/S brightness temperatures to minimize the bias in transitions between each instrument's imagery.

REFERENCES

Bovik, A. C., 2000: Basic gray-level image processing. *Handbook of Image and Video Processing,* A. C. Bovik, Ed., Academic Press, 21–36.

Cecil, D. J., and E. J. Zipser, 1999: Relationships between tropical cyclone intensity and satellite-based indicators of inner core convection: 86-GHz ice-scattering signature and lightning. *Mon. Wea. Rev.,* **127,** 103–123.

Corbosiero, K. L., and J. Molinari, 2002: The effects of vertical wind shear on the distribution of convection in tropical cyclones. *Mon. Wea. Rev.,* **130,** 2110–2123.

Fortner, L. E., 1958: Typhoon Sarah, 1956. *Bull. Amer. Meteor. Soc.,* **39,** 633–639.

Germann, U., and I. Zawadzki, 2002: Scale-dependence of the predictability of precipitation from continental radar images. Part I: Description of the methodology. *Mon. Wea. Rev.,* **130,** 2859–2873.

Grody, N. C., 1993: Remote sensing of the atmosphere from satellites using microwave radiometry. *Atmospheric Remote Sensing by Microwave Radiometry,* M. A. Janssen, Ed., John Wiley, 259–334.

Grose, A., E. A. Smith, H.-S. Chung, M.-L. Ou, B.-J. Sohn, and F. J. Turk, 2002: Possibilities and limitations for quantitative precipitation forecasts using nowcasting methods with infrared geosynchronous satellite imagery. *J. Appl. Meteor.,* **41,** 763–785.

Hawkins, J. D., T. F. Lee, J. Turk, C. Sampson, J. Kent, and K. Richardson, 2001: Real-time Internet distribution of satellite products for tropical cyclone reconnaissance. *Bull. Amer. Meteor. Soc.,* **82,** 567–578.

Hohti, H., J. Koistinen, P. Nurmi, E. Saltikoff, and K. Holmund, 2000: Precipitation nowcasting using radar-derived atmospheric motion vectors. *Phys. Chem. Earth B,* **25,** 1323–1327.

Holland, G. J., 1980: An analytic model of the wind and pressure profiles in hurricanes. *Mon. Wea. Rev.,* **108,** 1212–1218.

Houze, R. A., and Coauthors, 2006: The hurricane rainband and intensity change experiment: Observations and modeling of hurricanes Katrina, Ophelia, and Rita. *Bull. Amer. Meteor. Soc.,* **87,** 1503–1521.

Jones, T. A., D. Cecil, and M. DeMaria, 2006: Passive-microwave-enhanced statistical hurricane intensity prediction scheme. *Wea. Forecasting,* **21,** 613–635.

Joyce, R. J., J. E. Janowiak, P. A. Arkin, and P. Xie, 2004: CMORPH: A method that produces global precipitation estimates from passive microwave and infrared data at high spatial and temporal resolution. *J. Hydrometeor.,* **5,** 487–503.

Kummerow, C., W. Barnes, T. Kozu, J. Shiue, and J. Simpson, 1998: The Tropical Rainfall Measuring Mission (TRMM) sensor package. *J. Atmos. Oceanic Technol.,* **15,** 809–817.

Lee, T. F., F. J. Turk, J. Hawkins, and K. Richardson, 2002: Interpretation of TRMM TMI images of tropical cyclones. *Earth Interactions,* **6.** [Available online at http://EarthInteractions.org.]

NASA, MSFC, cited 2001: AMSR-E data management plan—August 2001. [Available online at www.ghcc.msfc.nasa.gov/AMSR/data_management_plan.html.]

NOAA OSDPD, cited 2002: General SSMIS information. [Available online at www.osdpd.noaa.gov/PSB/IMAGES/ssmisdoc.htm.]

Raytheon, cited 2000: SSM/I user's interpretation guide. 104 pp. [Available online at https://www.fnmoc.navy.mil/PUBLIC/SATELLITE/TUTORIAL/ssmi.pdf.]

Rozoff, C. M., W. H. Schubert, B. D. McNoldy, and J. P. Kossin, 2006: Rapid filamentation zones in intense tropical cyclones. *J. Atmos. Sci.,* **63,** 325–340.

Ruprecht, D., and H. Müller, 1995: Image warping with scattered data interpolation. *IEEE Comput. Graphics Appl.,* **15,** 37–43.

Spencer, R. W., H. M. Goodman, and R. E. Hood, 1989: Precipitation retrieval over land and ocean with the SSM/I: Identification and characteristics of the scattering signal. *J. Atmos. Oceanic Technol.,* **6,** 254–273.

Willoughby, H. E., J. A. Clos, and M. G. Shoreibah, 1982: Concentric eyewalls, secondary wind maxima, and the evolution of the hurricane vortex. *J. Atmos. Sci.,* **39,** 395–411.

Wohlberg, G., 1998: Image morphing: A survey. *Visual Comput.,* **14,** 360–372.